ARTECLE

J. Cent. South Univ. (2019) 26: 1493−1502
DOI: https://doi.org/10.1007/s11771-019-4105-8

Springer

Facile synthesis of $Sb@Sb_2O_3$/reduced graphene oxide composite with superior lithium-storage performance

ZHOU Xiao-zhong(周小中)[1], LU He-jie(陆和杰)[1], TANG Xing-chang(唐兴昌)[2], ZENG Ya-ping(曾娅萍)[1], YU Xin(余欣)[1]

1. Key Laboratory of Eco-Environment-Related Polymer Materials of Ministry of Education, Key Laboratory of Polymer Materials of Gansu Province, College of Chemistry and Chemical Engineering, Northwest Normal University, Lanzhou 730070, China;
2. State Key Laboratory of Gansu Advanced Non-ferrous Metal Materials, School of Materials Science and Engineering, Lanzhou University of Technology, Lanzhou 730050, China

Abstract: Sb-based materials have been considered one of the most promising anode electrode materials for lithium-ion batteries, whereas they were commonly synthesized through time-consuming and costly processes. Here, $Sb@Sb_2O_3$/reduced graphene oxide ($Sb@Sb_2O_3$/rGO) composite was successfully synthesized by a facile one-pot chemical method at ambient temperature. Based on the XRD and TGA analysis, the mass fractions of Sb and Sb_2O_3 in the $Sb@Sb_2O_3$/rGO composite are ca. 34.05% and 26.6%, respectively. When used as an alternative electrode for lithium ion batteries, a high reversible capacity of 790.9 mA·h/g could be delivered after 200 cycles with the capacity retention of 93.8% at a current density of 200 mA/g. And a capacity of 260 mA·h/g could be maintained even at 2000 mA/g. These excellent electrochemical properties can be attributed to its well-constructed nanostructure. The Sb and Sb_2O_3 particles with size of 10 nm were tightly anchored on rGO sheets through electronic coupling, which could not only alleviate the stress induced by the volume expansion, suppress the aggregation of Sb and Sb_2O_3 particles, but also improve the electron transfer ability during cycling.

Key words: $Sb@Sb_2O_3$/rGO composite; synthesis; electrochemical performance; lithium-ion batteries

Cite this article as: ZHOU Xiao-zhong, LU He-jie, TANG Xing-chang, ZENG Ya-ping, YU Xin. Facile synthesis of $Sb@Sb_2O_3$/reduced graphene oxide composite with superior Lithium-storage performance [J]. Journal of Central South University, 2019, 26(6): 1493−1502. DOI: https://doi.org/10.1007/s11771-019-4105-8.

1 Introduction

With the rapid development of society, more and more attention is being paid to the environmental protection and sustainable development, thus cleaner energy resources, such as solar and wind, have been extensively developed. To peak shift operation for these cleaner energy application, energy storage systems (ESSs) are requisite. Due to their high energy density, excellent cycling stability and low-toxicity, lithium ion batteries (LIBs) have been widely applied in portable electronic products, and become the primary candidates for automotive application and ESSs [1]. However, the commercial LIBs with graphite-based anode electrode are unable to meet those new applications considering the lower

Foundation item: Project(51462032) supported by the National Natural Science Foundation of China; Project(17JR5RA066) supported by the Foundation for Distinguished Young Scholars of Gansu Province, China
Received date: 2018-11-19; **Accepted date:** 2019-02-18
Corresponding authors: ZHOU Xiao-zhong, PhD, Associate Professor; Tel: +86-15117182652; E-mail: zxz20004@163.com; ORCID: 0000-0001-5366-0545; TANG Xing-chang, PhD, Lecturer; Tel: +86-13609359216; E-mail: tangxingchang@sohu.com; ORCID: 0000-0001-7934-9376

theoretical specific capacity (372 mA·h/g) of graphite [2]. Therefore, it is imperative to explore substitute electrodes with high specific capacity and long cycle life [3, 4].

Among those alternative anode materials, antimony-based materials have been considered one of the most promising anode electrode materials, attributed to their high theoretical capacity (Sb, 660 mA·h/g; Sb_2O_3, 1103 mA·h/g) [5], as well as appropriate kinetic and voltage characteristics which could effectively prevent the emergence of lithium dendrites [6]. Before practical application in LIBs, several issues such as low practical specific capacity and poor cycling stability should be solved properly. The low practical specific capacities can be due to the low utilization of the active materials and/or the partly irreversible conversion reaction of antimony-based compounds during cycling. Large volume changes during the de-lithiation/lithiation reactions cause the electrode fracture and pulverization [7], as well as the continuous growth of solid electrolyte interphase (SEI) film, resulting in rapid capacity fading [8]. Partial reduction of antimony-based compound to form Sb/Sb_2O_3 composite can relieve the stress induced by volume expansion, which is beneficial to improve its cycling stability [8, 9]. YANG et al [8] synthesized the Sb/Sb_2O_3@C spheres through a partial reduction method, which delivers a good capacity of 467 mA·h/g after 95 cycles. Formation of nano-sized active materials and carbonaceous modification can greatly enhance their electrochemical performance [10−14]. The nano-sized active materials could enhance the electrochemical reaction kinetics owe to their unique surface microstructure, and promote the reversible reactions [3, 15−17]. With superior electronic conductivity, stable chemical properties and huge specific surface area [18], graphene has been widely used in high-performance LIBs [19, 20]. In our previous reported work, anchoring Sb_2O_3 [10], Sb_2O_4 [11] and Sb_6O_{13} [12] nanoparticles on reduced graphene oxide (rGO) sheets by a solvothermal method could improve the reversible capacities and electrochemical stabilities to a large extent, which can be attributed to the synergistic effect of the rGO sheets and the nano-sized antimony oxides. The interactions between active antimony oxides and the rGO sheets supporter can effectively inhibit nanoparticles aggregation and enhance the electrical conductivity, resulting in the superior electrochemical performance.

However, these antimony-based materials with excellent electrochemical performance are commonly synthesized through time-consuming and costly processes. Here, a facile one-pot chemical reduction method has been employed to synthesize $Sb@Sb_2O_3$/rGO composite at ambient temperature, using Sb_2O_3 as antimony source, graphene oxide (GO) as supporter, ethylene glycol as solvent, and $NaBH_4$ as reductive agent. As verified, 10 nm Sb and Sb_2O_3 nanoparticles are tightly anchored on rGO sheets. When used for LIBs application, the as-obtained $Sb@Sb_2O_3$/rGO composite could deliver a high reversible capacity of 790.9 mA·h/g after 200 cycles at a current density of 200 mA/g, corresponding to the capacity retention of 93.8%.

2 Experimental

2.1 Synthesis of GO, $Sb@Sb_2O_3$ and $Sb@Sb_2O_3$/rGO composite

Graphene oxide (GO) was prepared by a modified Hummers' method [4], using natural flake graphite as raw material. The obtained GO aqueous solution (0.1 mg/mL) was freeze-dried for further use. $Sb@Sb_2O_3$/rGO composites were synthesized by a facile one-pot chemical reduction method, as shown in Figure 1. Typically, 1 g of Sb_2O_3 was ultrasonically dispersed in 100 mL ethylene glycol (EG) for 0.5 h. The obtained mixture solution was heated and further stirred at 110 °C for 0.5 h and during which ethylene glycol antimony compound was formed as a result of the reaction between EG and Sb_2O_3 [21]. After being cooled down to ambient temperature, 2.0 g of freeze-dried GO (FDGO) was added and dispersed ultrasonically. Finally, excess $NaBH_4$ ethanol solution was dropwise added into above mixed suspension and continuously stirred for another 1.5 h. The precipitate was collected by extraction filtration and washed sequentially with ethanol and distilled water, and then dried in an oven at 80 °C to obtain $Sb@Sb_2O_3$/rGO composite. As for comparison, $Sb@Sb_2O_3$ composite and bare rGO were also synthesized by the same process except for the addition of FDGO and Sb_2O_3, respectively.

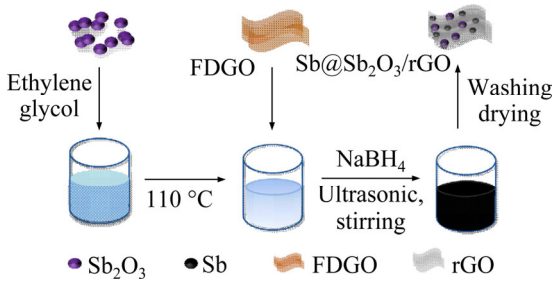

Figure 1 Schematic illustration of synthesis procedure for Sb/Sb_2O_3/rGO sample

2.2 Material characterization

Field-emission scanning electron microscope (FE-SEM, Ultra Plus, Carl Zeiss, Germany,) and field-emission transmission electron microscope (TEM, FEI TECNAI TF20) were employed to investigate the microstructures of the samples. The phase compositions were identified by X-ray diffraction (XRD, PANalytical Empyrean) using Jade 5.0 of Material Data, Inc. (MDI). The surface structure was analyzed by X-ray photoelectron spectra (XPS, PHI-5702, Al K_α X-ray radiation). A Pyris Diamond thermogravimetric analyzer (TGA, PrekinElmer, U.S.A.) was used to determine the Sb and Sb_2O_3 contents of $Sb@Sb_2O_3$/rGO composite, which was operated between room temperature and 800 °C with a heating rate of 10 °C/min under ambient atmosphere.

2.3 Electrochemical characterizations

Electrochemical lithium-storage properties of the as-obtained samples were evaluated through cyclic voltammetry (CV) and galvanostatic charge−discharge (GSCD) measurements in the voltage range of 0.01−3.0 V vs Li^+/Li at ambient temperature, using 2025-type coin cells in an argon-filled glovebox. The electrical conductivities were measured by electrochemical impedance spectroscopy (EIS). The GSCD measurements were performed on a battery testing system (CT2001A, Wuhan LAND Electronics Co., Ltd., China). On an electrochemical workstation (Autolab PGSTAT128N, Metrohm, Switzerland), the CV curves were obtained at a scan rate of 0.2 mV/s, as well as the EIS curves obtained over a frequency range of 10^{-5}−10^2 kHz at open-circuit potentials. The 2025-type coin cells were assembled with lithium metal wafer as the counter electrode, a Celgard 2400 polypropylene foil as the separator, and 1 mol/L $LiPF_6$ solution in a dimethyl carbonate/ethyl methyl carbonate/ethylene carbonate (DMC/EMC/EC, 1:1:1 by volume) mixture as the electrolyte. For the testing electrode, the active powder materials, polyvinylidene fluoride and carbon black were mixed together and magnetically stirred with a mass ratio of 75:15:10 to form a homogeneous slurry, and then blade coated on copper foil substrate. After vacuum-dried at 80 °C overnight, the as-prepared electrodes were cut into discs with a diameter of 10 mm for 2025-type coin cells. The specific capacities were calculated based on the total weight of as-obtained composites.

3 Results and discussion

3.1 Structure, morphology and composition of $Sb@Sb_2O_3$/rGO composite

Figure 2(a) shows the XRD patterns of the obtained $Sb@Sb_2O_3$ and $Sb@Sb_2O_3$/rGO composites. Obviously, the intense diffraction peaks in both samples can be well indexed to the elemental Sb phase with rhombohedral structure (JCPDS card No. 85-1322), as well as several weak peaks for senarmontite cubic structured Sb_2O_3 phase (JCPDS card No. 05-0534), indicating the successful reduction of Sb^{3+} into Sb^0 and successful synthesis of $Sb@Sb_2O_3$ composite by the facile one-pot chemical reduction method at ambient temperature. According to the semi-quantitative analysis with the as-known reference intensity value (K) of the characteristic diffraction peaks, the mass ratio of Sb to Sb_2O_3 is about 7.47 and 1.28 in $Sb@Sb_2O_3$ and $Sb@Sb_2O_3$/rGO, respectively. The relative higher Sb_2O_3 content in $Sb@Sb_2O_3$/rGO composite can be attributed to the addition of GO, which could play a role of weak oxidant [12]. A wide diffraction peak located at around 2θ=25.2° originated from rGO can be detected, indicating the successful reduction of GO [22]. To further verify the reduction of GO, Raman spectroscopy was employed. As shown in Figure 2(b), compared with bare GO and rGO, the higher integrated intensity ratio of characteristic D band and G band (I_D/I_G= 1.25) for $Sb@Sb_2O_3$/rGO composite indicates higher reduction degree for rGO in composite than that for bare rGO [12, 23], which is beneficial for electric conductivity and lithium storage properties [24, 25]. Moreover, a tiny peak located at 146 cm^{-1} can be attributed to the A_{1g} band of the Sb phase, indentifying the presence of Sb in the

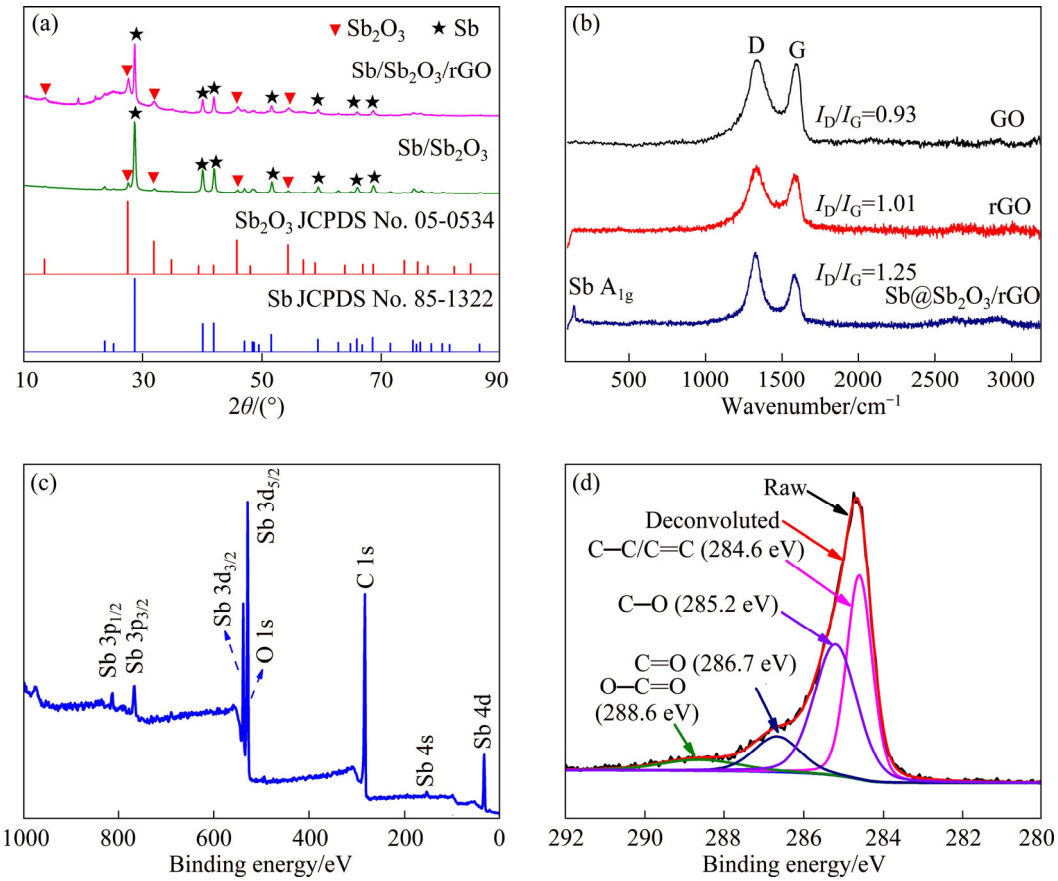

Figure 2 XRD patterns of $Sb@Sb_2O_3$ and $Sb@Sb_2O_3/rGO$ nanoparticles (a), Raman spectra of GO, rGO and $Sb@Sb_2O_3/rGO$composite (b), full XPS spectrum (c) and high-resolution C 1s XPS spectra of $Sb@Sb_2O_3/rGO$composite (d)

as-synthesized $Sb@Sb_2O_3/rGO$ composite.

The surface structure of the obtained $Sb@Sb_2O_3/rGO$ composite was analyzed by XPS measurement. Figure 2(c) displays the full XPS spectrum for $Sb@Sb_2O_3/rGO$ composite, in which only three elements (C, O and Sb) can be detected, confirming that element Sb is present in the $Sb@Sb_2O_3/rGO$ composite [26, 27]. Figure 2(d) displays the bonding information of C 1s investigated by means of XPS peak-differenating analysis. It can be seen that, the high-resolution XPS spectra of C 1s can be fitted well with four peaks at 288.6, 286.7, 285.2 and 284.6 eV, which are assigned to O—C═O, C═O, C—O, and C—C/C═C, respectively [28]. And the relative weak intensities of the O—C═O and C═O peaks further confirm that GO has been reduced into rGO after the facile one-pot chemical reduction procedure at ambient temperature, which agrees well with the results of XRD and Raman analysis [10, 29]. It is surprising that the binding energy of C—O (285.2 eV) is much lower than that of the standard C—OH, indicating that there is a strong electronic coupling between rGO sheets and Sb/Sb_2O_3 particles in the $Sb@Sb_2O_3/rGO$ composite [30]. This strong electronic coupling could enhance the electron transfer ability and suppress the aggregation of active particles during de-/lithiation process, leading to excellent electrochemical performance [10, 12, 31].

The mass fraction of $Sb@Sb_2O_3$ in the composite $Sb@Sb_2O_3/rGO$ was estimated by TGA measurement. As shown in Figure 3, a slight mass loss of 7.6 wt% from room temperature to 180 °C is mainly due to evaporation of water that adsorbed on the surface of the sample [32]. The major mass loss of 52.0% from 180 °C to 625 °C is associated with multiple factors, mainly including the volatilization and oxidation of Sb and Sb_2O_3 to form Sb_2O_4 [10, 30], and combustion of the rGO component in the air [33]. According to the XRD and TGA results, the mass fractions of Sb and Sb_2O_3 in the as-synthesized $Sb@Sb_2O_3/rGO$ composite are 34.0% and 26.6%, respectively.

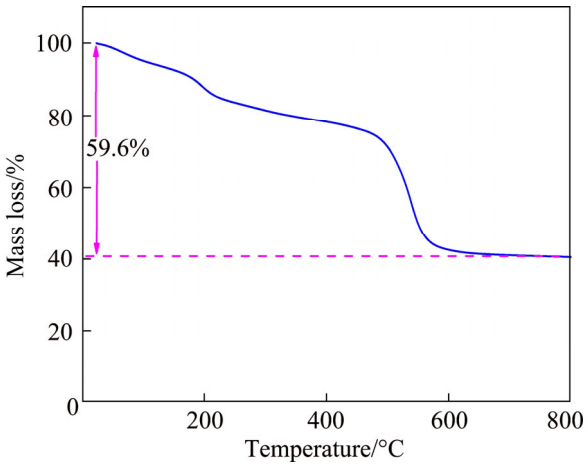

Figure 3 Thermogravimetric analysis (TGA) curve of as-obtained Sb@Sb_2O_3/rGO composite

The microstructure characteristics of Sb@Sb_2O_3 and Sb@Sb_2O_3/rGO composites were investigated using SEM and TEM technologies. As shown in Figure 4(a), the Sb and/or Sb_2O_3 particles in size of ca. 50 nm (inset in Figure 4(a)) aggregate together to form porous structure. The obtained Sb@Sb_2O_3/rGO composite displays a bulk with stacked layer structure, and no obvious particles can be observed (Figure 4(b)). According to the element mappings inset in Figure 4(b), three elements C, O and Sb are evenly distributed in the composite, indicating that Sb and Sb_2O_3 particles are uniformly dispersed in obtained Sb@Sb_2O_3/rGO composite. Figure 4(c) and (d) shows the TEM observations for Sb@Sb_2O_3/rGO composite, in which particles in size of ca. 10 nm were uniformly dispersed in rGO sheets. The inserted selected area electron diffraction (SAED) in Figure 4(c) displays the diffraction rings characteristic of Sb and Sb_2O_3. Moreover, the high-resolution TEM image of the composite (Figure 4(d)) shows two phases that can be identified as rhombohedral Sb with interplanar spacing of 0.184 nm for (012) plane and cubic Sb_2O_3 with interplanar spacing of 0.279 nm for (400) plane, respectively, further revealing that both Sb and Sb_2O_3 nanoparticles were anchored firmly on rGO sheets. And these results are consistent with the analysis of XRD.

The strong interaction effect between rGO sheets and Sb/Sb_2O_3 particles can be also confirmed

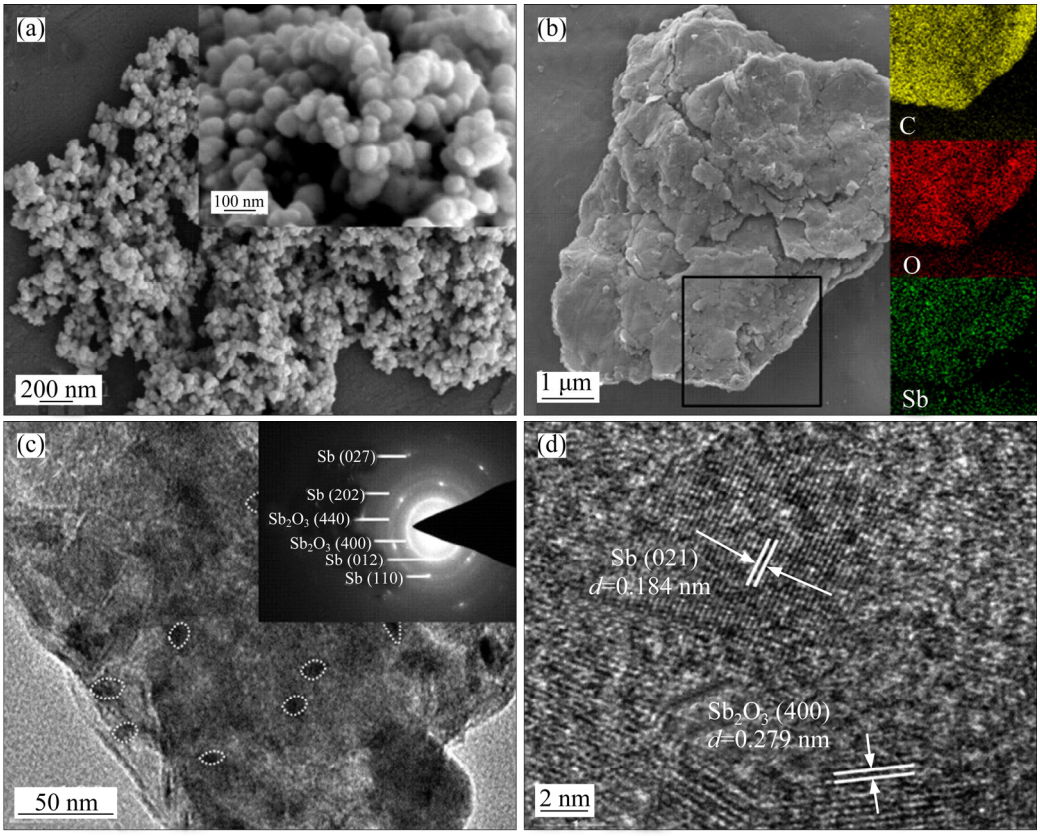

Figure 4 FE-SEM images of Sb@Sb_2O_3 (a) and Sb@Sb_2O_3/rGO composites (b), TEM (c) and high-resolution TEM (d) images of Sb@Sb_2O_3/rGO composite (Corresponding magnified image, EDS mapping, and selected area electron diffraction (SAED) pattern are insets in panel (a), (b) and (c), respectively)

through the EIS measurement of the assembled half cells. The EIS curves among bare Sb_2O_3, $Sb@Sb_2O_3$ and $Sb@Sb_2O_3$/rGO composite are compared in Figure 5. All EIS curves of samples show a semicircle relating to the charge transfer resistance (R_{ct}) in the medium and high frequency region, as well as a gradient line representing the lithium ion diffusion process in the low frequency region [12, 34]. Distinctly, the obtained $Sb@Sb_2O_3$/rGO composite shows smallest R_{ct} value than those for bare Sb_2O_3 and $Sb@Sb_2O_3$ composite, confirming the enhanced electrical contact between rGO sheets and $Sb@Sb_2O_3$ particles by strong electric coupling, which is conducive to improving cycling ability.

3.2 Electrochemical properties of obtained samples for LIBs application

For LIBs application, electrochemical properties of the $Sb@Sb_2O_3$/rGO composite were evaluated by CV and GSCD tests in the voltage range of 0.01−3.0 V vs Li^+/Li at ambient temperature, as shown in Figure 5. Figure 5(a) displays the typical CV curves of the $Sb@Sb_2O_3$/rGO electrode in the initial three cycles at a scan rate of 0.2 mV/s. During the first cycling, a reduction peak located at ca. 1.15 V can be attributed to the reduction of Sb_2O_3 compound to form Li_2O and nano-sized Sb [10, 35], and another one at ca. 0.55 V is derived from the alloying of Sb to form Li_3Sb and the formation of solid electrolyte interface (SEI) film [10, 36, 37]. In subsequent cycles, the two reduction peaks shift to ca. 1.59 and 0.75 V, respectively, indicating an activation process during the first cycle [10], in which the primal Sb and/or Sb_2O_3 particles have been transferred into ones with smaller size after the first cycle [38], leading to improving the lithiation reaction kinetics. The reduction peak below 0.25 V originates from the insertion of lithium into rGO

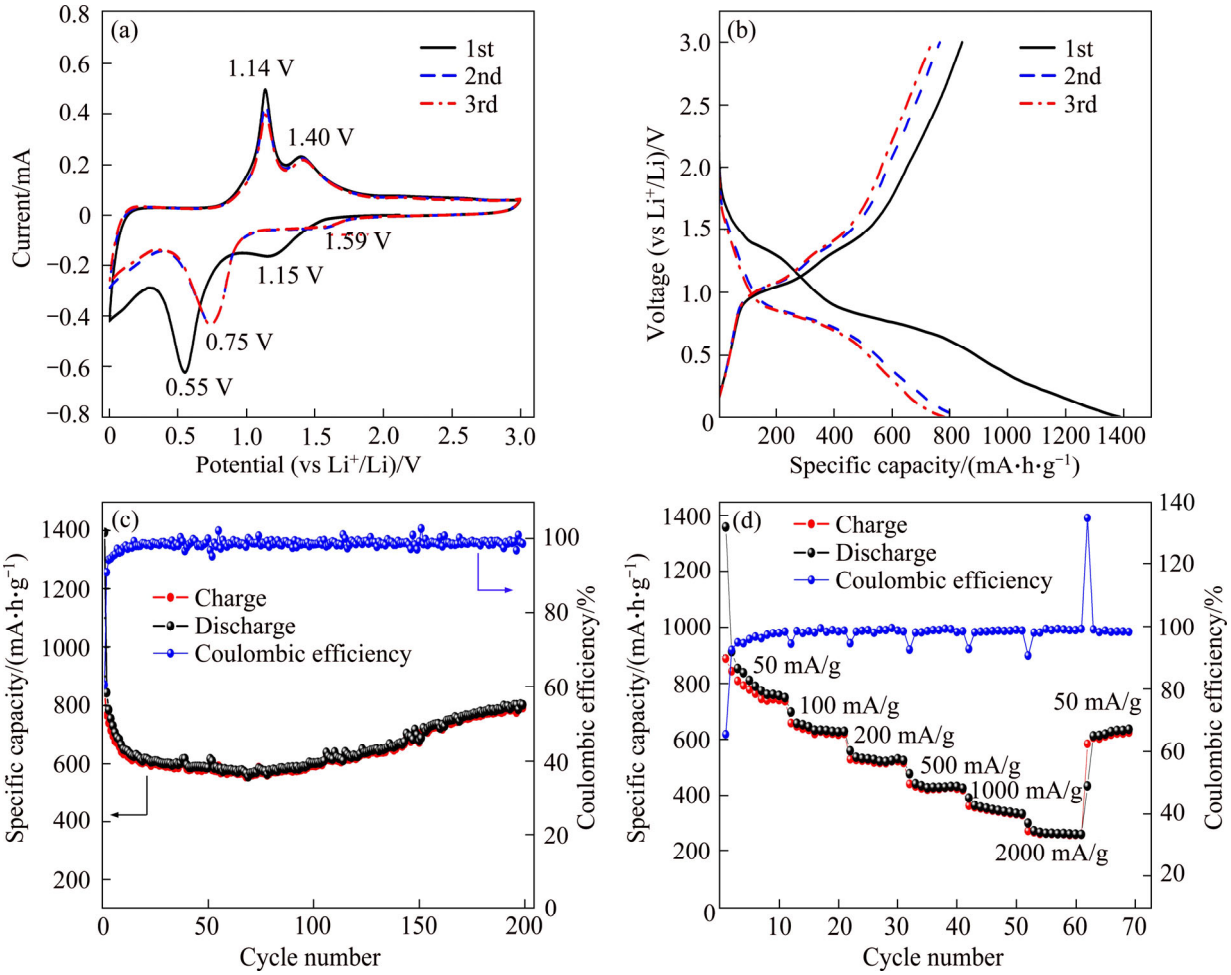

Figure 5 CV curves at a scan rate of 0.2 mV/s (a), galvanostatic charge−discharge profiles at a current density of 200 mA/g (b), cycling performance at 200 mA/g (c), and rate capability at various current densities of $Sb@Sb_2O_3$/rGO electrode (d)

sheets, in accordance with the alkali metal storage in those carbonaceous electrode [39]. During the charging process, two oxidation peaks located at 1.14 and 1.40 V are respectively owing to the reverse process of the alloying reaction and the reconstitution of Sb_2O_3 phase [10, 40], indicating a reversible conversion reaction between Sb and Sb_2O_3 during cycling ascribed to the strong interaction effect between rGO sheets and $Sb@Sb_2O_3$. Moreover, both redox peak pairs at 1.14/0.75 V and 1.40/1.59 V, respectively, corresponding to (de-)alloying and conversion lithium storage mechanism overlapped well during the subsequent cycles, suggesting a good electrochemical stability [41].

Moreover, all corresponding voltage plateaus were also detected in the GSCD curves of the $Sb@Sb_2O_3$/rGO electrode at a current density of 200 mA/g, as shown in Figure 5(b). There are two distinct voltage plateaus at around 1.3 and 0.7 V in the first discharge process corresponding to the reduction of Sb_2O_3 and the lithiation reaction of Sb and formation of SEI film, respectively, and a slant region below 0.5 V originating from the lithiation of rGO sheets. As well, two plateaus at around 1.0 and 1.4 V during the charge process can be detected for de-alloying reaction of Li_3Sb and reformation of Sb_2O_3. These reversible processes corresponding to (de)alloying and conversion reactions are in accordance with the CV results. The electrochemical cycling performance of the $Sb@Sb_2O_3$/rGO electrode has been tested at 200 mA/g for 200 cycles. A high initial reversible specific capacity of 843.5 mA·h/g with an initial coulombic efficiency of 60.6% can be delivered for the $Sb@Sb_2O_3$/rGO electrode at 200 mA/g. A rapid capacity fading to 633 mA·h/g in initial 10 cycles is ascribed to those unanchored $Sb@Sb_2O_3$ particles, which were pulverized due to large volume changing during the initial several cycles and further became inactive towards lithium. The fading can be relieved by optimizing technological process in the further investigations. It is noteworthy that, the capacity increased gradually since 70 cycles owing to the reversible formation of gel-like film [31]. And the reversible capacity of as high as 790.9 mA·h/g with the capacity retention of 93.8% could be maintained after 200 cycles (Figure 5(c)). The $Sb@Sb_2O_3$/rGO electrode also displays excellent rate capacities. As shown in Figure 5(d), the reversible capacities stabilized ca. 740, 620, 522, 425 and 330 mA·h/g at current densities of 50, 100, 200, 500 and 1000 mA/g, respectively. A high reversible capacity of 260 mA·h/g can be obtained even at 2000 mA/g. When the current density was returned to 50 mA/g, the reversible capacity can be fully recovered to above 638 mA·h/g after 10 cycles, indicating high structure stability and superior rate capability of the $Sb@Sb_2O_3$/rGO electrode. The above excellent lithium storage properties can be attributed to the well-constructed nanostructure. Sb and Sb_2O_3 particles in size of ca. 10 nm were tightly anchored on rGO sheets through electronic coupling, which could not only suppress the aggregation of active nanoparticles, alleviate the stress caused by the volume expansion, but also enhance the electron transfer ability during de-/lithiation process.

4 Conclusions

1) $Sb@Sb_2O_3$/rGO composite has been successfully synthesized by a facile one-pot chemical reduction method at ambient temperature.

2) As an alternative electrode for LIBs application, the as-synthesized $Sb@Sb_2O_3$/rGO composite delivers a high reversible capacity of 790.9 mA·h/g after 200 cycles with a capacity retention of 93.8% at 200 mA/g.

3) The excellent electrochemical properties can be attributed to the well-constructed nanostructure. The nano-sized Sb and Sb_2O_3 particles are tightly anchored on rGO sheets through electronic coupling, which could not only alleviate the stress caused by the volume expansion and suppress the aggregation of active nanoparticles, but also enhance the electron transfer ability during cycling.

4) And these findings are useful in synthesizing functional materials through facile and convenient method and developing novel and alternative electrode materials with high electrochemical performance for LIBs.

References

[1] TARASCON J M, ARMAND M. Issues and challenges facing rechargeable lithium batteries [J]. Nature, 2001,

414(6861): 359−367. DOI: 10.1038/35104644.

[2] ZHAO Yang, LI Xi-fei, YAN Bo, XIONG Dong-bin, LI De-jun, LAWES S, SUN Xue-liang. Recent developments and understanding of novel mixed transition-metal oxides as anodes in lithium ion batteries [J]. Advanced Energy Materials, 2016, 6(8): 1502175. DOI: 10.1002/aenm.201502175.

[3] WU Ling, ZHENG Jie, WANG Liang, XIONG Xun-hui, SHAO Yan-yan, WANG Gang, WANG Jeng-han, ZHONG Sheng-kui, WU Ming-hong. PPy-encapsulated SnS_2 nanosheets stabilized by defects on TiO_2 support as durable anode material for lithium-ion battery [J]. Angewandte Chemie International Edition, 2019, 58: 811−815. DOI: 10.1002/anie.201811784.

[4] XIONG Xun-hui, WANG Zhi-xing, YUE Peng, GUO Hua-jun, WU Fei-xiang, WANG Jie-xi, LI Xin-hai. Washing effects on electrochemical performance and storage characteristics of $LiNi_{0.8}Co_{0.1}Mn_{0.1}O_2$ as cathode material for lithium-ion batteries [J]. Journal of Power Sources, 2013, 222: 318−325. DOI: 10.1016/j.jpowsour.2012.08.029.

[5] YU D Y, PRIKHODCHENKO P V, MASON C W, BATABYAL S K, GUN J, SLADKEVICH S, MEDVEDEV A G, LEV O. High-capacity antimony sulphide nanoparticle-decorated graphene composite as anode for sodium-ion batteries [J]. Nature communications, 2013, 4(4): 1−7. DOI: 10.1038/ncomms3922.

[6] BAI Peng, LI Ju, BRUSHETT F R, BAZANT M Z. Transition of lithium growth mechanisms in liquid electrolytes [J]. Energy Environmental Science, 2016, 9(10): 3221−3229. DOI: 10.1039/c6ee01674j.

[7] WU Tian-jing, ZHANG Chen-yang, HOU Hong-shuai, GE Peng, ZOU Guo-qiang, XU Wei, LI Si-min, HUANG Zhao-dong, GUO Tian-xiao, JING Ming-jun, JI Xiao-bo. Dual functions of potassium antimony(III)-tartrate in tuning antimony/carbon composites for long-life Na-ion batteries [J]. Advanced Functional Materials, 2018, 28(10): 1705744. DOI: 10.1002/adfm.201705744.

[8] YANG Xia, MA Jing-jing, WANG Hui-jun, CHAI Ya-qin, YUAN-Ruo. Partially reduced Sb/Sb_2O_3@C spheres with enhanced electrochemical performance for lithium ion storage [J]. Materials Chemistry and Physics, 2018, 213: 208−212. DOI: 10.1016/j.matchemphys.2018.04.027.

[9] BRYNGELSSON H, ESKHULT J, NYHOLM L, HERRANEN M, ALM O, EDSTRÖ K. Electrodeposited Sb and Sb/Sb_2O_3 nanoparticle coatings as anode materials for Li-ion batteries [J]. Chemistry of Materials, 2007, 19(5): 1170−1180. DOI: 10.1021/cm0624769.

[10] ZHOU Xiao-zhong, ZHANG Zheng-feng, LU Xiao-fang, LV Xue-yan, MA Guo-fu, WANG Qing-tao, LEI Zi-qiang. Sb_2O_3 Nanoparticles anchored on graphene sheets via alcohol dissolution-reprecipitation method for excellent lithium-storage properties [J]. ACS Applied Materials & Interfaces, 2017, 9(40): 34927−34936. DOI: 10.1021/acsami.7b10107.

[11] ZHOU Xiao-zhong, ZHANG Zheng-feng, WANG Jian-wen, WANG Qing-tao, MA Guo-fu, LEI Zi-qiang. Sb_2O_4/reduced graphene oxide composite as high-performance anode material for lithium ion batteries [J]. Journal of Alloys and Compounds, 2017, 699: 611−618. DOI: 10.1016/j.jallcom.2016.12.434.

[12] ZHOU Xiao-zhong, ZHANG Zheng-feng, XU Xiao-hu, YAN Jian, MA Guo-fu, LEI Zi-qiang. Anchoring Sb_6O_{13} nanocrystals on graphene sheets for enhanced lithium storage [J]. ACS Applied Materials & Interfaces, 2016, 8(51): 35398−35406. DOI: 10.1021/acsami.6b13548.

[13] ZHOU Jing, ZHENG Cai-hong, WANG Hua, YANG Jie, HU Peng-fei, GUO Lin. 3D nest-shaped Sb_2O_3/RGO composite based high-performance lithium-ion batteries [J]. Nanoscale, 2016, 8(39): 17131−17135. DOI: 10.1039/c6nr06454j.

[14] XUE Xia, SUN Dan, ZENG Xian-guang, HUANG Xiao-bing, ZHANG He-he, TANG You-gen, WANG Hai-yan. Two-step carbon modification of $NaTi_2(PO_4)_3$ with improved sodium storage performance for Na-ion batteries [J]. Jounal of Central South University, 2018, 25: 2320−2331. DOI: 10.1007/s11771-018-3916-3.

[15] POIZOT P, LARUELLE S, GRUGEON S, DUPONT L, TARASCON J M. Nano-sized transition-metal oxides as negative-electrode materials for lithium-ion batteries [J]. Nature, 2000, 407: 496−499. DOI: 10.1038/35035045.

[16] ZHANG Rui, LI Hui-yong, SUN Dan, LUAN Jing-yi, HUANG Xiao-bing, TANG You-gen, WANG Hai-yan. Facile preparation of robust porous MoS_2/C nanosheet networks as anode material for sodium ion batteries [J]. Jounal of Materials Science, 2019, 54: 2472−2482. DOI: 10.1007/s10853-018-2991-z.

[17] SUN Dan, ZHU Xiao-bo, LUO Bin, ZHANG Yu, TANG You-gen, WANG Hai-yan. New binder-free metal phosphide-carbon felt composite anodes for sodium-ion battery [J]. Advanced Energy Materials, 2018, 8: 1801197. DOI: 10.1002/aenm.201801197.

[18] XIONG Dong-bin, LI Xi-fei, SHAN Hui, YAN Bo, DONG Li-tian, CAO Ye, LI De-jun. Controllable oxygenic functional groups of metal-free cathodes for high performance lithium ion batteries [J]. Journal of Materials Chemistry A, 2015, 3(21): 11376−11386. DOI: 10.1039/C5TA01574J.

[19] WU Song-ping, XU Rui, LU Ming-jia, GE Rong-yun, IOCOZZIA J, HAN Cui-ping, JIANG Bei-bei, LIN Zhi-qun. Graphene-containing nanomaterials for lithium-ion batteries [J]. Advanced Energy Materials, 2015, 5(21): 1500400. DOI: 10.1002/aenm.201500400.

[20] JI Li-wen, MEDURI P, AGUBRA V, XIAO Xing-cheng, ALCOUTLABIl M. Graphene-based nanocomposites for energy storage [J]. Advanced Energy Materials, 2016, 6(16): 1502159. DOI: 10.1002/aenm.201502159.

[21] ZHOU Xiao-zhong, ZHANG Zheng-feng, LV Xue-yan, AN Chun-yang, MA Guo-fu, LEI Zi-qiang. Facile and rapid synthesis of Sb_2O_3/CNTs/rGO nanocomposite with excellent sodium storage performances [J]. Materials Letters, 2018, 213: 201−203. DOI: 10.1016/j.matlet.2017.11.059.

[22] DREYER D R, PARK S, BIELAWSKI C W, RUOFF R S. The chemistry of graphene oxide [J]. Chemical Society Reviews, 2010, 39(1): 228−240. DOI: 10.1039/b917103g.

[23] NITHYA C, GOPUKUMAR S. RGO/nano Sb composite: A high performance anode material for Na^+ ion batteries and

evidence for the formation of nanoribbons from the nano rGO sheet during galvanostatic cycling [J]. Journal of Materials Chemistry A, 2014, 2(27): 10516−10525. DOI: 10.1039/c4ta01324g.

[24] OU Xing, YANG Cheng-hao, XIONG Xun-hui, ZHENG Feng-hua, PAN Qi-chang, JIN Chao, LIU Mei-lin, HUANG K. A new rGO-overcoated Sb_2Se_3 nanorods anode for Na^+ battery: In situ X-ray diffraction study on a live sodiation/desodiation process [J]. Advanced Functional Materials, 2017, 27(13): 1606242. DOI: 110.1002/adfm.201606242.

[25] ZHU Xiao-ming, LI Qian, FANG Yong-jin, LIU Xiao-ling, XIAO Li-fen, AI Xin-ping, YANG Han-xi, CAO Yu-liang. Graphene-modified TiO_2 microspheres synthesized by a facile spray-drying route for enhanced sodium-ion storage [J]. Particle & Particle Systems Characterization, 2016, 33(8): 545−552. DOI: 10.1002/ppsc.201500216.

[26] HERNÁNDEZ-RENTERO C, VARGA O, CABALLERO A, MORALES J, MARTÍN F. Solvothermal-induced 3D graphene networks: Role played by the structural and textural properties on lithium storage [J]. Electrochimica Acta, 2016, 222: 914−920. DOI: 10.1016/j.electacta.2016.11.057.

[27] XU Xin, SI Ling, ZHOU Xiao-si, TU Feng-zhang, ZHU Xiao-shu, BAO Jian-chun. Chemical bonding between antimony and ionic liquid-derived nitrogen-doped carbon for sodium-ion battery anode [J]. Journal of Power Sources, 2017, 349: 37−44. DOI: 10.1016/j.jpowsour.2017.03.026.

[28] HU Mei-juan, JIANG Yin-zhu, SUN Wen-ping, WANG Hong-tao, JIN Chuan-hong, MI Yan. Reversible conversion-alloying of Sb_2O_3 as a high-capacity, high-rate, and durable anode for sodium ion batteries [J]. ACS Applied Materials & Interfaces, 2014, 6(21): 19449−19455. DOI: 10.1021/am505505m.

[29] DARWICHE A, BODENES L, MADEC L, MONCONDUIT L, MARTINEZ H. Impact of the salts and solvents on the SEI formation in Sb/Na batteries: An XPS analysis [J]. Electrochimica Acta, 2016, 207: 284−292. DOI: 10.1016/j.electacta.2016.03.089.

[30] SLADKEVICH S, GUN J, PRIKHODCHENKO P V, GUTKIN V, MIKHAYLOV A A, MEDVEDEV A G, TRIPOL'SKAYA T A, LEV O. The formation of a peroxoantimonate thin film coating on graphene oxide (GO) and the influence of the GO on its transformation to antimony oxides and elemental antimony [J]. Carbon, 2012, 50(15): 5463−5471. DOI: 10.1016/j.carbon.2012.07.033.

[31] ZHOU Xiao-si, WAN Li-jun, GUO Yu-guo. SnO_2 nanocrystals in nitrogen-doped graphene sheets as anode materials for lithium-ion batteries [J]. Advanced Materials, 2013, 25(15): 2152−2157. DOI: 10.1002/adma.201300071.

[32] WANG Gui-zhi, FENG Jian-min, DONG Lei, LI Xi-fei, LI De-jun. Porous graphene anchored with Sb/SbO_x as sodium-ion battery anode with enhanced reversible capacity and cycle performance [J]. Journal of Alloys and Compounds, 2017, 693: 141−149. DOI: 10.1016/j.jallcom.2016.09.150.

[33] HOU Hong-shuai, YANG Ying-chang, ZHU Yi-rong, JING Ming-jun, PAN Cheng-chi, FANG Lai-bing, SONG Wei-xin, YANG Xu-ming, JI Xiao-bo. An electrochemical study of Sb/acetylene black composite as anode for sodium-ion batteries [J]. Electrochimica Acta, 2014, 146: 328−334. DOI: 10.1016/j.electacta.2014.09.080.

[34] GUO Qi, ZHENG Zhe, GAO Hai-ling, MA Jia, QIN Xue. SnO_2/graphene composite as highly reversible anode materials for lithium ion batteries [J]. Journal of Power Sources, 2013, 240(31): 149−154. DOI: 10.1016/j.jpowsour.2013.03.116.

[35] XUE Ming-zhe, FU Zheng-wen. Electrochemical reaction of lithium with nanostructured thin film of antimony trioxide [J]. Electrochemistry Communications, 2006, 8(8): 1250−1256. DOI: 10.1016/j.elecom.2006.04.022.

[36] WU Ya-nan, PAN Qi-chang, ZHENG Feng-hua, OU Xing, YANG Cheng-hao, XIONG Xun-hui, LIU Mei-lin, HU Dong-li, HUANG Chun-lai. Sb@C/expanded graphite as high-performance anode material for lithium ion batteries [J]. Journal of Alloys and Compounds, 2018, 744: 481−486. DOI: 10.1016/j.jallcom.2018.02.049.

[37] WANG Zhen-zhen, QU Jin, HAO Shu-meng, ZHANG Yu-jiao, KONG Fan-qiang, YANG Dong-zhi, YU Zhong-zhen. Sb nanoparticles embedded in nitrogen-doped carbon matrix with tuned voids and interfacial bonds for high-rate lithium storage [J]. ChemElectroChem, 2018, 5(18): 2653−2659. DOI: 10.1002/celc.201800781.

[38] YI Zheng, HAN Qi-Gang, ZAN Ping, WU Yao-ming, CHENG Yong, WANG Li-min. Sb nanoparticles encapsulated into porous carbon matrixes for high-performance lithium-ion battery anodes [J]. Journal of Power Sources, 2016, 331: 16−21. DOI: 10.1016/j.jpowsour.2016.09.027.

[39] WANG Gang, XIONG Xun-hui, XIE Dong, LIN Zhi-hua, ZHENG Jie, ZHENG Feng-hua, LI You-peng, LIU Yan-zhen, YANG Cheng-hao, LIU Mei-lin. Chemically activated hollow carbon nanospheres as a high-performance anode material for potassium ion batteries [J]. Journal of Materials Chemistry A, 2018, 6: 24317−24323. DOI: 10.1039/c8ta09751h.

[40] JIN Ren-cheng, JIANG Hua, WANG Qing-yao, LI Gui-hua, GAO Shan-min. Sb nanoparticles anchored on nitrogen-doped amorphous carbon-coated ultrathin CoS_x nanosheets for excellent performance in lithium-ion batteries [J]. ACS Applied Materials & Interfaces, 2017, 9(51): 44494−44502. DOI: 10.1021/acsami.7b14280.

[41] ZHOU Xiao-si, DAI Zhi-hu, BAO Jian-chun, GUO Yu-guo. Wet milled synthesis of an Sb/MWCNT nanocomposite for improved sodium storage [J]. Journal of Materials Chemistry A, 2013, 1: 13727−13731. DOI: 10.1039/C3TA13438E.

(Edited by FANG Jing-hua)

中文导读

具有优越储锂性能的 $Sb@Sb_2O_3$/还原氧化石墨烯复合材料的简易制备

摘要：锑基材料被认为是制备锂离子电池最具应用前景的负极材料之一，然而复杂而成本昂贵的制备过程严重限制了其应用。本文采用一锅化学还原的简便方法在室温下得到 $Sb@Sb_2O_3$/还原氧化石墨烯($Sb@Sb_2O_3$/rGO)复合材料。XRD 和 TGA 结果表明，复合材料中 Sb 和 Sb_2O_3 的质量分数分别为 34.0%和 26.6%。将该复合材料用作锂离子电池电极材料使用时，在 200 mA/g 电流密度下循环 200 次后可逆比容量仍保持在 790.9 mA·h/g，容量保持率高达 93.8%；在 2000 mA/g 电流密度下充放电时仍有 260 mA·h/g 的可逆比容量。优越的电化学性能得益于所制备复合材料良好的纳米结构，尺寸约为 10 nm 的 Sb 和 Sb_2O_3 颗粒通过电子耦合作用牢牢地锚定在还原氧化石墨烯片层上。该结构既能有效缓冲因储锂过程中产生体积膨胀而引起的应力作用，还可抑制 Sb 和 Sb_2O_3 纳米颗粒的团聚，更能提高活性材料的导电性。

关键词：$Sb@Sb_2O_3$/rGO 复合材料；制备；电化学性能；锂离子电池